A quantitative approach of extracting magnetic moments in small cylindrical object

C-Y. Hsieh[1], Y-C. N. Cheng[1], J. Neelavalli[1], and E. M. Haacke[1]

[1]Wayne State University, Detroit, Michigan, United States

Introduction: Susceptibility is key to revealing information about oxygenation saturation levels, calcium and iron. We have developed a complex sum method that can be used to determine magnetic susceptibility of narrow but long cylinders from MR images (see Eq. 1) [1]. Our previous studies of the complex sum method [1] required the knowledge of the object size. In this abstract, we present an improved approach that determines the effective magnetic moment without any *a priori* information.

Theory and Methods: An air cylinder in a gel phantom was previously imaged by a 3D gradient-echo sequence [1]. With the same imaging parameters and orientation, we simulated an air cylinder surrounded by water with $B_0 = 1.5$T, TE 5ms and 20ms [1-3]. The air cylinder was perpendicular to B_0 [1-3]. The radius of the air cylinder (a) was 0.8 mm and image resolutions (Δx and Δy) were 1 mm. The magnetic susceptibility difference between water and air was assumed to be -9.4 ppm in SI unit [4] so the effective magnetic moment is defined as $\boldsymbol{p} \equiv \boldsymbol{g}\boldsymbol{a}^2$ where g is defined as $0.5\gamma B_0 \Delta\chi TE$, γ is the gyromagnetic ratio, $2\pi \cdot 42.58$ MHz/T, and $\Delta\chi$ is the magnetic susceptibility between air and water. Therefore, ***p*** was -6.03 rad·mm^2 and -24.1 rad·mm^2 at TE 5ms and 20ms, respectively. The black dot shown in Fig. 1 at the center of the magnitude image represents the cross section of the cylinder. Eq.1 shows the overall complex MR signal S_i summed up within a circle of radius R_i (as any of the circles in Fig. 1). The overall complex MR signal happens to be a real number in the case of a cylindrical object. For this reason the center of the cylinder can be determined [1]. With three concentric circles shown in Fig. 1, re-arrangement of Eq.1 leads to Eq.2 in which ***p*** becomes the only unknown. Because the maximum phase value (θ_i) at the *i*-th circle outside the phase aliasing region is $\boldsymbol{p}/R_i^2$ in Eq.2, if this maximum phase value is chosen to be less than 2.4 rad, then ***p*** can be uniquely determined. We also studied the uncertainty of ***p*** in the presence of both systematic (discretization) and thermal noise through error propagation (Eq.3) [2]. These two noise sources are uncorrelated. Eq. 3 tells us for what imaging parameters and R_i the uncertainty of ***p*** may be the least. Moreover, the phase profile from an image slice was similar to Fig. 2(b). With the proper choice of R_i, their corresponding phase values are listed in Table 1. We measured ***p*** from the air cylinder in the simulations and different slices of the gel images. The ***p*** values of the air cylinder in different slices at both TE 5 and 20ms are listed in Table 2. The uncertainties of ***p*** in columns 3 and 5 in Table 2 were estimated from Eq.3.

$$S_i = \pi l \rho_0 p \int_{p/R_i^2}^{g} dx \frac{J_0(x)}{x^2} \quad \text{—(1)} \qquad (S_1 - S_2) \times \int_{p/R_2^2}^{p/R_3^2} dx \frac{J_0(x)}{x^2} = (S_2 - S_3) \times \int_{p/R_1^2}^{p/R_2^2} dx \frac{J_0(x)}{x^2} \quad \text{———————(2)}$$

$$\frac{\delta p}{p} = \frac{\sqrt{|h_1 - h_2|^2 \left| \frac{\Delta x \Delta y}{\pi SNR^2}(R_2^2 - R_3^2) \right| + p^2 \varepsilon_{12}^2 (h_2 - h_3)^2 + |h_2 - h_3|^2 \left| \frac{\Delta x \Delta y}{\pi SNR^2}(R_1^2 - R_2^2) \right| + p^2 \varepsilon_{23}^2 (h_1 - h_2)^2}}{\left| J_0(p/R_3^2) R_3^2 (h_1 - h_2) + J_0(p/R_2^2) R_2^2 (h_3 - h_1) + J_0(p/R_1^2) R_1^2 (h_2 - h_3) \right|} \quad (3)$$

Notations in equations: The effective magnetic moment p is defined as the above. ρ_0 and l are the spin density of water (including imaging parameters) and length of the cylinder, respectively. J_0 is the Bessel function. In Eq.3, ε_{ij} is the systematic noise (error) in each annual region, which can be estimated from Table 1.

Table 1: Error estimation of ***p*** in the simulation		
TE = 5 ms	Phases (3, 2, 1)	Phases (2.4, 1.4, 1)
Systematic noise	0.3%	4.8%
Thermal noise only	2.6%	5.8%
TE = 20 ms	Phases (3, 2, 1)	Phases (2.4, 1.4, 1)
Systematic noise	0.4%	2.7%
Thermal noise only	1.3%	2.4%

Phase unit: rad, SNR=14.5 and tube radius=1 pixel

Table 2 Gel data analysis at TE 5 and 20 ms

Slice TE:ms	$\boldsymbol{p_1}$ 5ms	$\delta\boldsymbol{p_1}/\boldsymbol{p_1}$ (%)	$\boldsymbol{p_2}$ 20ms	$\delta\boldsymbol{p_2}/\boldsymbol{p_2}$ (%)	$\boldsymbol{p_3}$ 20ms	$\boldsymbol{p_2}$ vs $\boldsymbol{p_3}$ (%)
10	-6.93	6	-26.1	2	-27.7	6
19	-6.06	14	-23.7	9	-24.2	2
28	-5.96	13	-21.0	7	-23.8	12
37	-4.82	15	-18.3	9	-19.3	5
43	-4.27	6	-17.8	5	-17.1	4

$\boldsymbol{p_i}$ unit: rad-mm^2 $\boldsymbol{p_3} = \boldsymbol{p_1} \times 4$; a=0.8 mm

Results: Most results show an uncertainty of ***p*** less than 10% [3]. For the uncertainty study in Table 1, the uncertainty of ***p*** decreases from $(\theta_1,\theta_2,\theta_3)=(2.4,1.4,1)$ to $(\theta_1,\theta_2,\theta_3)=(3,2,1)$ at two different TEs. At echo time, 20 ms, the uncertainty of ***p*** is less than that at the TE 5ms. These results are predicted by Eq.3. Eq. 3 implies that a longer echo time and a high signal noise ratio could lead to accurate ***p*** of the small cylinder. In Table 2, $\boldsymbol{p_3}$ is calculated from $\boldsymbol{p_1}$ and is the expected magnetic moment at TE 20ms. For the same slice of the gel phantom, ***p*** values at TE 5 and 20ms agree with each other within uncertainties (Table 2). As predicted by Eq. 3, in the same slice, the uncertainty of ***p*** at TE 20ms is also less than that at TE 5ms shown in Table 2.

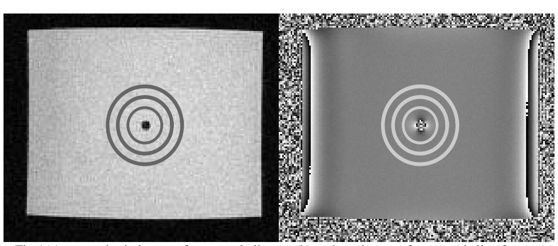

Fig.1(a) a magnitude image of a coronal slice (b) a phase image of a coronal slice from an air cylinder in a gel phantom with an in-plane resolution of 1x1 mm^2 and TE 20ms.

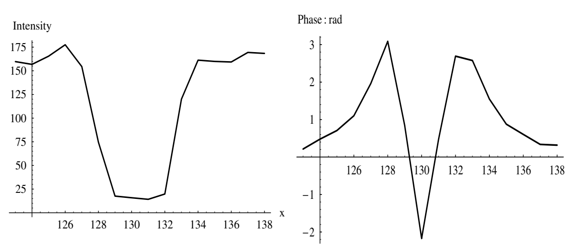

Fig. 2 (a) central magnitude profile in Fig. 1. (b) central phase profile in Fig. 1

Discussions and Conclusion: Results in Table 2 indicate that the air cylinder may slightly collapse at the bottom slice so its radius may be smaller. Simulations with a variety of cylinder radii support this conclusion. The simulations and experimental results well agree with each other. This outcome indicates a promising potential of this method.

References: [1] Cheng et al. M.R.I. 2007; p.1171-1180. [2] Hsieh et al. Medical Physics 2007; p. 2358. [3] Hsieh et al. Proc. ISMRM 2007; p. 2596. [4] Robson et al. AIChE journal 2005; p. 1633-1640